2019 Fourteenth International Conference on Ecological Vehicles and Renewable Energies (EVER)

Connected-Autonomous Electric Vehicles based on DC-Bus Stabilisation Using Hybrid Storage System

T. C. Lin, S. A. Amamra, and J. Marco
International Digital Laboratory, Warwick Manufacturing Group
Coventry, CV4 7AL, U.K.
Email: t.lin.3@warwick.ac.uk, sidali.amamra@warwick.ac.uk, james.marco@warwick.ac.uk

***Abstract*—This paper proposes a novel DC-bus voltage control technique for a connected-autonomous electric vehicle (CAEV) using a hybrid supercapacitor-battery energy storage system. The verification by simulation of the control system that manages the current flow from the supercapacitor by using a rule-based algorithm within a CAEV is described. A feedforward compensator is included within the control scheme to suppress DC-bus voltage excursions under highly variable driveline torque conditions. Furthermore, the proposed control system has been verified by the case of CAEV being subject to a real-world driving cycle and acceleration/deceleration modes in order to reflect realistic electric vehicle powertrain operations.**

Keywords*—*Autonomous electric vehicle, battery, electric vehicle, feedback and feedforward control, hybrid energy storage system, power converter, and supercapacitor.

I. INTRODUCTION

New energy vehicles, e.g. electric vehicles (EVs) have received mass attention since they have the advantages of improving the energy crisis and pollution in the environment such as no fuel consumption, reduced daily traveling costs and little noise [1]. Many automotive companies are showing various models of EVs with better performance and improved driving distance, such as Nissan, BMW, and Jaguar Land Rover. The performance of EVs, such as driving range, acceleration/braking, and dynamic attributes, all depend on the performances of the powertrain components such as the electrical machine, the inverter, the battery or the battery in combination with the supercapacitor (SC) as a hybrid energy storage system. Considering the battery has a high-energy capacity while a relatively low power density and the SC has much higher power densities and extremely high cycling capability with less maintenance, a hybrid energy storage system (HESS) can provide both high power density and high energy capacities [2][3]. SC-Battery HESS provides some advantages such as 1) improvement of the battery life; 2) improvement in power management; 3) SC can recover more energy from the regenerative braking [4].

In this paper, a cascaded control system is developed for the enhancement of the DC-bus voltage stabilization. In the control system, the SC is connected to the DC-bus via a bi-directional DC-DC converter and controlled by a rule-based controller. This leads to the reduced complexity of the control scheme than other topologies which can be implemented more easily. Meanwhile, the relationship between the frequency response and the stability of DC-bus voltage during periods of vehicle acceleration and regenerative braking are investigated and discussed. The final outputs of the control algorithm are applied in a Matlab/Simulink environment for off-line simulation-based verification. The paper is structured as follows: the introduction and works related to control strategies for HESS-based electric vehicles are discussed in Section I. Section II focuses on the behavioral based models for HESS. This is followed by the architecture of CAEV in Section III. The control approaches to the HESS are explained in Section IV. Section V discusses the analysis of simulation performances. The overall conclusions are given in Section VI.

II. MODELS OF HYBRID ENERGY STORAGE SYSTEM

This section describes a behavioral based SC model, battery model, and power electronics converter. The descriptions of the modelling concepts are described in the following subsections.

A. Model of Supercapacitor

The SC is a high-power density energy storage device with a much higher recharging cycle than batteries. It has a very fast dynamic response in charging and discharging. The output voltage of SC simultaneously reaches its steady

state when it switches from maximum charging current to the maximum discharging current [5]. Within the linear working region, the SC can be model by a fixed value of capacitance and equivalent series resistance accurately without considering the effect by the temperature and other operation conditions [6]. Fig. 1 shows a simple RC circuit model performing as the SC model.

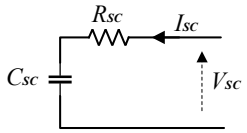

Fig. 1. Equivalent circuit model of SC [7].

The Kirchhoff's Voltage Law (KVL) mathematical equation model is derived as

$$V_{SC} = I_{SC} \cdot R_{SC} + V_{C_{SC}} \tag{1}$$

where V_{SC} is the terminal voltage of SC, I_{SC} is the SC current, C_{SC} and R_{SC} are the capacitance and equivalent series resistor of SC. V_{SC} can be represented as

$$V_{SC} = C_{SC} \frac{dV_{C_{SC}}}{dt} V_{co} \cdot R_{SC} + V_{C_{SC}} \tag{2}$$

Based on (1) and (2), the model can be rearranged as

$$\frac{dV_{SC}}{dt} - R_{SC} \frac{dI_{SC}}{dt} = -\frac{1}{C_{SC}} I_{SC} \tag{3}$$

In Fig. 2 (a), a current pulse is applied to the SC model, and the output of voltage response is shown in Fig. 2 (b). The voltage of SC varies between 54V to 37V which is set as the upper and lower limits during the operation. The bode plots of SC is obtained and shown in Fig. 2 (c).

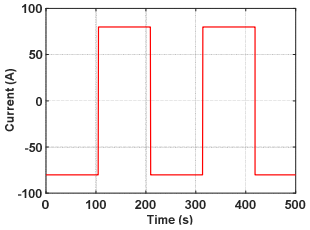

(a) Variation of current pulse

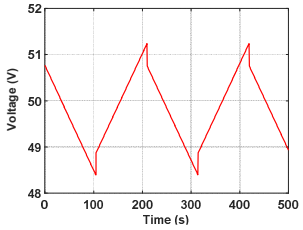

(b) Variation of voltage

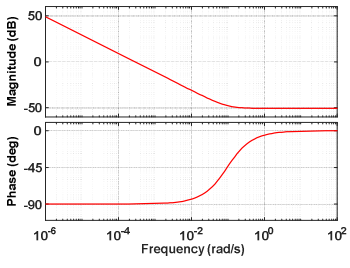

(c) Bode plot (Input = current, I_{SC}, output = voltage, V_{SC}).

Fig. 2. Performance of SC.

B. *Model of Battery*

The electrical models of the battery can be divided into two categories: the low-power application that neglects the thermal effect, and the high-power application that includes the impact of temperature in the battery performance [8]. The terminal voltage of a battery is presented from the Thevenin battery model depending on the open circuit voltage (OCV) V_{ocv}, and the internal resistance R_i [9] and the paralleled RC circuit as shown in Fig. 3.

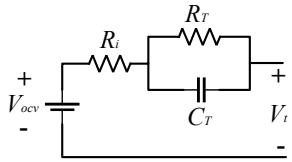

Fig. 3. Equivalent circuit model of battery.

The battery transient behavior corresponding to the load change is represented by the resistance R_T with a paralleled capacitor C_T. The battery OCV is depended on its actual state of charge (SoC) with a non-linear equation. This term represents a voltage that changes with the amplitude of the current and the actual charge of the battery [10]. The cell voltage calculations are done using an equivalent circuit model as the dynamic model of the battery which is presented as [11]

$$V_t = V_{OCV} - R_i \cdot I - V_{CR} \Rightarrow V_{CR} = V_{OCV} - R_i \cdot I - V_t \tag{4}$$

$$\frac{dV_{CR}}{dt} = -\frac{V_{CR}}{RC} + \frac{1}{C} \cdot I \tag{5}$$

where V_t and V_{OCV} are the terminal voltage and the open circuit voltage of the battery, respectively. Besides, the battery aging is not considered in this paper, which decreases the battery fully charged capacity. Substitute (4) into (5), the dynamic model of the battery can be re-written as

$$\frac{d}{dt}V_{OCV} - R_i \frac{d}{dt} I - \frac{d}{dt} V_t = -\frac{1}{RC} V_{OCV} + \frac{R_i}{RC} I + \frac{1}{RC} V_t + \frac{1}{C} \cdot I \tag{6}$$

The SoC is defined as the ratio between the charge left in a battery and its rated capacity, and the SoC is presented as

$$SoC = SoC_{\text{int}} + \frac{1}{3600 A_{bat}} \int Idt \tag{7}$$

where SoC_{int} is the initial SoC of the battery, I is the battery current, and A_{bat} is the capacity of the battery.

The relationship between SoC and OCV is shown in Fig. 4. Similarly, a current pulse is also applied to the battery model (Fig. 5 (a)), and the output of the voltage

response is shown in Fig. (b). It also shows how the battery voltage varies between 55V to 35V. In Fig. 5 (c), the Bode plots of SC is obtained based on the different SoC conditions.

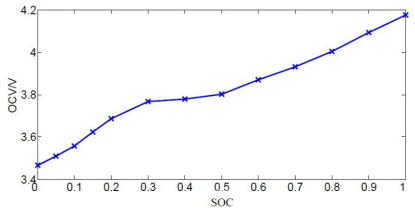

Fig. 4. Relationship of SoC and OCV.

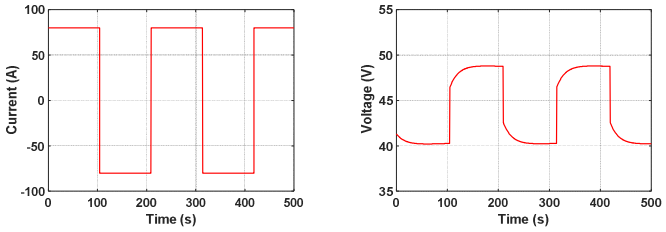

(a) Variation of current pulse (b) Variation of voltage

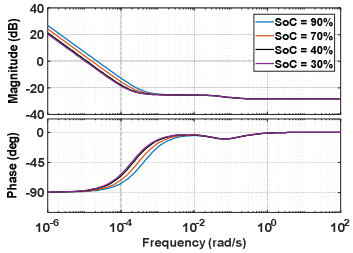

(c) Bode plot (Input = current, I, output = voltage, V_t)

Fig. 5. Performance of battery.

C. *Model of Power Electronics Converter*

In Fig. 6, the four-switch bi-directional DC-DC converter is employed which composes of an inductor, a capacitor and four power switches [12].

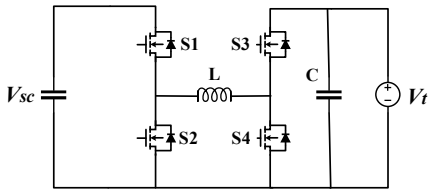

Fig. 6. Circuit diagram of bi-directional DC-DC converter.

By comparing the input voltage (V_{SC}) and the DC-bus voltage (V_t), the current flow direction can be determined. The current transfer can then be realized by controlling the power switches. The charging/discharging mode here is defined as the energy transferring from the DC-bus/input voltage to the input voltage/DC-bus (buck-boost or boost-buck). Using the time average model [12], the mathematical equation of the power electronics converter is written as:

Buck mode: $S_1 = S_4 = \text{ON}, \quad S_2 = S_3 = \text{OFF}$

$$\begin{cases} L\dfrac{di_L}{dt} = V_{SC} \\ C\dfrac{dV_t}{dt} = -\dfrac{V_t}{R} \end{cases} \Rightarrow \begin{cases} \dfrac{di_L}{dt} = \dfrac{1}{L}V_{SC} \\ \dfrac{dV_t}{dt} = -\dfrac{1}{CR}V_t \end{cases} \tag{8}$$

Boost mode: $S_1 = S_4 = \text{OFF}, \quad S_2 = S_3 = \text{ON}$

$$\begin{cases} L\dfrac{di_L}{dt} = -V_{SC} \\ C\dfrac{dV_t}{dt} = i_L - \dfrac{1}{R}V_t \end{cases} \Rightarrow \begin{cases} \dfrac{di_L}{dt} = -\dfrac{1}{L}V_{SC} \\ \dfrac{dV_t}{dt} = -\dfrac{1}{C}i_L - \dfrac{1}{R}V_t \end{cases} \tag{9}$$

The time average model of the complete operational model with physical variables and parameters can be written as

$$\begin{cases} \dfrac{di_L}{dt} = -\dfrac{1}{L}(1-D_2)V_t + \dfrac{1}{L}D_1V_{SC} \\ \dfrac{dV_t}{dt} = \dfrac{1}{C}(1-D_2)i_L - \left(\dfrac{1}{CR}D_1 + \dfrac{1}{R}(1-D_2)\right)V_t \end{cases} \tag{10}$$

The converter dynamic analysis for a buck-boost converter output voltage with the above setting from the time average model and circuitry models is shown in Fig. 7 as well as the Bode plot shown in Figs. 7 (c) and (d). It shows the converter dynamic behavior which is vital for DC-DC converter closed loop controller design. For example, to test the functionality of the converter, the time average model simulation gives a theoretical output voltage of 20V to 55V. The circuitry model simulates the output of 55V. Again, it can be clearly seen that both models output are almost overlapped with each other, except the time average model is not able to simulate the ripple effect on the output voltage.

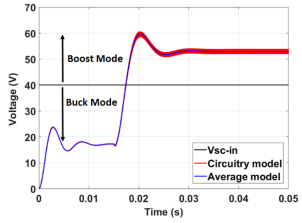

(a) Variation of output voltage

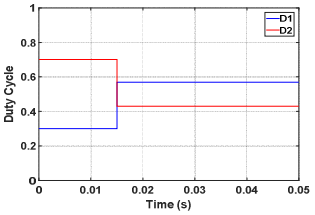

(b) Duty cycle

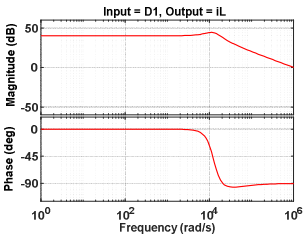

(c) Buck mode

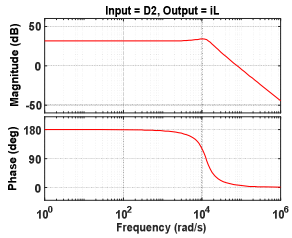

(d) Boost mode

Fig. 7. Performance of bi-directional converter, buck-boost mode.

III. ARCHITECTURE OF CAEV

The architecture of CAEV shown in Fig. 8 is studied in this paper. A single electrical motor is coupled to a differential transmission that drives the front wheels. The controllers are responsible for managing the power flow between the available drive systems. The figure also defines the power source that will fulfill the energy requested by the electrical motor. The HESS used is composed of an SC together with a bi-directional DC-DC converter associated with a battery.

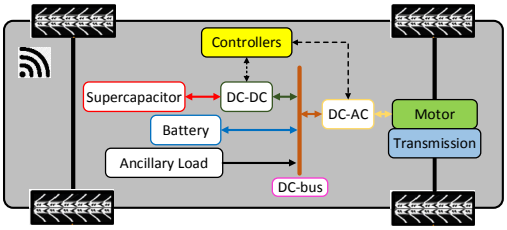

Fig. 8. Architecture of CAEV.

IV. DC-BUS CONTROL STRATEGIES FOR CAEV

In this section, the feedback and feedforward rule-based control schemes for HESS are aiming to improve the dynamic performance of CAEV. Within the context of the control strategies, the electrical machines behave as an external disturbance to the feedback control loop. The integration of the bi-directional DC-DC converter for the SC provides the energy management strategy with a "degree-of-freedom" to manage the current that is sourced to the DC-bus voltage. After the completion of the control process, the performance of the control strategies is therefore investigated and evaluated.

More importantly, the objectives of the control approaches are 1) to bias the current management towards the SC to highlight its use and potential application; 2) to stabilize the DC-bus voltage; 3) to minimize current flows between the battery and SC to maximize efficiency. The details will be described in the following subsections.

A. Design of DC-Bus Feedback Control

The standard feedback control loop sometimes does not provide good enough performance for the processes with long time delays and strong disturbances. Cascade control loops can be utilized and are a common feature in the process control industries for the control of temperature, flow, and pressure loops. In this paper, a cascade control structure [13] with a fast-inner current loop and an outer voltage loop for managing the current flow within the CAEV is shown in Fig. 9 [9]. The DC-bus voltage is regulated by the outer loop via the SC and battery currents which is tightly controlled by a faster inner loop. It is obvious that the SC reference current is produced from the outer voltage loop of the controller. This is done after a reference DC-bus voltage subtracting from the actual DC-bus voltage. The reference signal is passed to the inner current control loop if its value does not exceed the SC current produced by the control system. After passing the boundary limit block, the current demand is subtracted from the real output SC current then the error signal is treated as the duty cycle (D) for the bi-directional DC-DC converter, which is limited between (0-1).

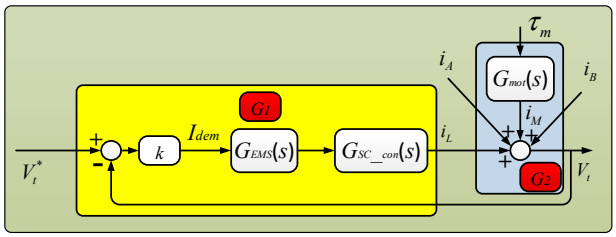

Fig. 9. Structure of the feedback control system.

As mentioned, the inner current loop is to provide the duty cycle signal for controlling the bi-directional buck-boost DC-DC converter for there to be a negligible steady-state error in response to a step input. According to the control theory [14], the error of the system can be reduced by increasing the gain in the open-loop system or using higher order systems. However, the system stability and dynamic performances are also influenced by either the large gain of the open-loop system or if the order of the system is too high.

The rule-based logic strategy offers good solutions to the power split problems in electric vehicles because of their flexibility and robustness. In this work, the current demand (I_{dem}) supplied by the energy storage system (i.e. load leveling) is determined based on some pre-defined rules as shown in Fig. 10. When the current demand is obtained, it will be used as the input signal to the energy management system which is also based on the pre-defined rules as shown in Fig. 11.

In this way, the supercapacitor SoC can be decreased to the min-max variation range quickly and thus guarantee the SC to work within the reasonable capacity fluctuation range. If the supercapacitor SoC drops down to its lower limit value, the battery is considered to share the load current to avoid the large drop of the supercapacitor SoC. When the battery SoC is bigger than its minimum value, the load current is distributed to battery only. It must be noted that the described rules above mainly include three work modes for the SC and

battery: 1) the battery work only; 2) the SC work only; 3) the battery and SC working together. In fact, when the SC exceeds the min-max supercapacitor SoC variation range, the load current is distributed to battery and SC jointly. In this process, the charge is also carried out simultaneously.

```
function I_dem = CA(Set_point_Voltage, DC_Bus_Volt)

k = 300;   % Proportional gain;

if DC_Bus_Volt < Set_point_Voltage      % Postive current for discharging;

    I_dem = (Set_point_Voltage - DC_Bus_Volt)*k;

elseif DC_Bus_Volt > Set_point_Voltage  % Negative current for Charging;

    I_dem = (Set_point_Voltage - DC_Bus_Volt)*k;

else

    I_dem = 0;

end
```

Fig. 10. Simple logic control for current demand calculation, I_{dem}.

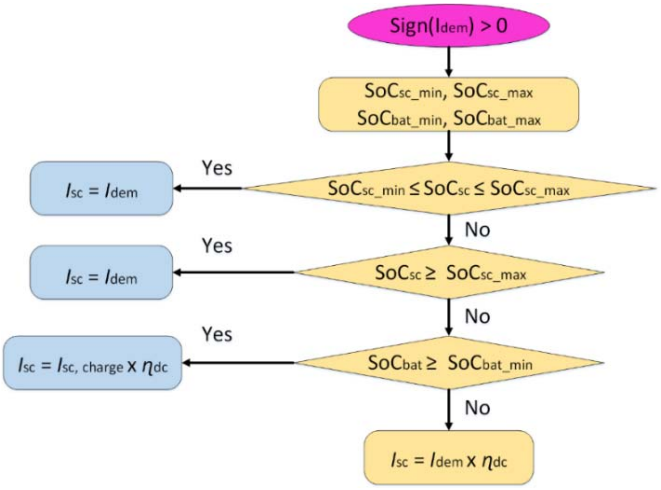

Fig. 11. Flowchart of driving condition control mode, G_{EMS}.

To obtain the current i_L, the equation can be derived as

$$i_L = I_{dem} \cdot G_{EMS}(s) \cdot G_{SC\_con}(s) \tag{11}$$

$$I_{dem} = V_t^* - V_t \cdot k \tag{12}$$

where i_L is the current of the bi-directional DC-DC converter. I_{dem} is the current demand for the rule-based energy management system. G_{EMS} is the rule-based logic controller (Fig. 11) for the energy management system. G_{SC_con} is the supercapacitor and the bi-directional DC-DC converter. V_t^* and V_t are the set-point voltage and the feedback DC-bus voltage. k is the proportional gain for current demand calculation.

$$i_{bus} = i_L \pm i_M \pm i_B \pm i_A \tag{13}$$

where i_{bus} is the total DC-bus current. i_M, i_B, and i_A are the currents of the electrical machine, the battery, and ancillary load, respectively.

The transfer function of the feedback control system can be obtained as

$$V_t = V_t^* \cdot G_1(S) + \tau_m \cdot G_2(S) \tag{14}$$

$$G_1 = I_{dem} \cdot G_{EMS}(s) \cdot G_{SC\_con}(s) \tag{15}$$

$$G_2 = G_{mot}(s) \tag{16}$$

According to the concept of the control, the regulated DC-bus voltage should be equal to the upper bound when the vehicle is a standstill for an expected acceleration. In addition, the demanded DC-bus voltage should be equal to the lower bound when the vehicle at full speed, so the regenerative should be captured in the SC from the next expected step which is deceleration or breaking.

B. Design of DC-Bus Feedforward Compensator

As mentioned, the disturbance signal or transient error may deteriorate the performance at steady and dynamic states. However, it can be improved by a feedforward control method. Hence, the combined feedback-feedforward control technique can significantly improve the overall performance over simple feedback control whenever there is a major disturbance that can be measured before it affects the process output. In the most ideal situation, feedforward control can entirely eliminate the effect of the measured disturbance on the process output. Even when there are modelling errors, feedforward control can often reduce the effect of the measured disturbance on the output better than that achievable by feedback control alone. Feedforward control is always used along with feedback control because a feedback control system is required to track set-point changes and to suppress unmeasured disturbances that are always present in any real process as shown in Fig. 12.

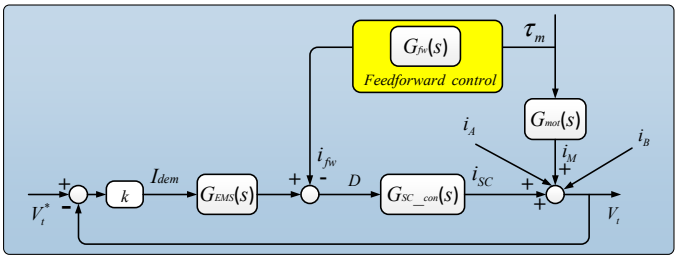

Fig. 12. Structure of feedback and feedforward control system.

The main objective of the feedforward control is designed to cancel out the main dynamics of the inner current control system (i.e. the current drawn from the SC equals the current drawn by the machine). The following expressions for the control process variable are given as:

$$i_{SC} = i_M \Rightarrow i_B = 0 \text{ (ideal situation)} \tag{17}$$

where i_{SC} is the SC current reflected the DC-bus current. Based on (3.4), the transfer function of the feedforward control loop can be obtained as

$$G_{fw}(s) = G_{mot}(s) \cdot G_{SC\_con}^{-1}(s) \tag{18}$$

The DC bus load current is reconstructed based on the known traction motor torque reference τ_m and torque current i_{fw} reference relationship.

$$i_{fw} = \alpha \cdot G_{fw}(s) \cdot \tau_m \tag{19}$$

where the scaling factor α is chosen as a trade-off between fast response and noise suppression.

Figs. 13 show the responses of feedforward current and feedback voltage based on the different scale factor. It is observed that the feedback control system improves the response of the output using a bigger scale factor of the feedforward compensator as drawn in Fig. 13 (b). The reason for the degradation in response is that the controller attempts to suppress the disturbance signal, created by the feedforward compensator. However, the response of the controller is long enough with respect to the settling time of the feedback loop that the feedback loop is capable of diminishing the effect of the disturbance on the output. It is evidenced that the disturbance current signal can be canceled when the feedforward control method is applied as shown in Fig. 13 (a). The voltage drop in the feedback DC-bus voltage (Fig. 13 (b)) has successfully been compensated.

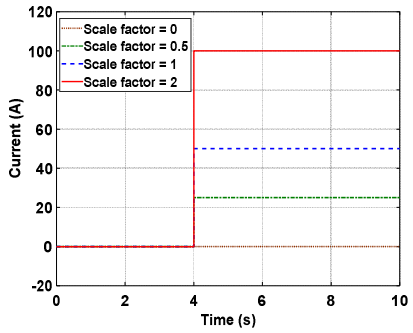

(a) Feedforward current (i_{fw})

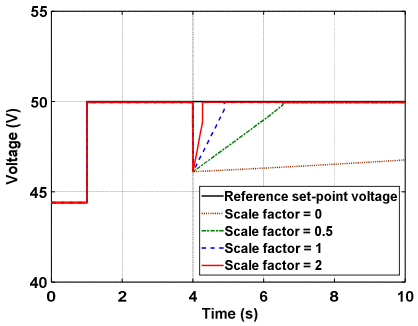

(b) Feedback voltage (V_t)

Fig. 13. Comparison of different scale factors.

V. Analysis of Simulation Performance

The DC bus control strategy has been verified by means of simulation analysis based on the electric vehicle dynamic model subjected to the CAEV driving cycles and acceleration/deceleration regimes. The overall structure of a control scheme for the DC-bus voltage control system based on an energy management system and a feedforward compensator is shown in Fig. 14.

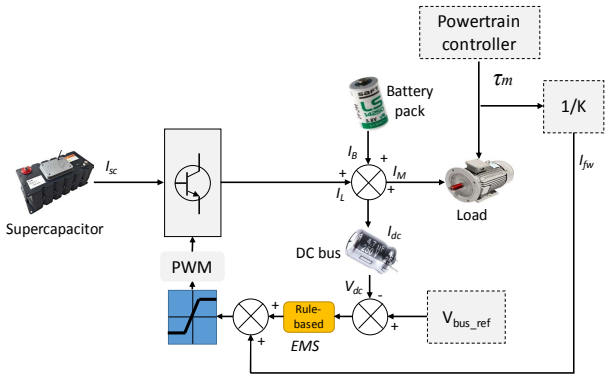

Fig. 14. The overall structure of control scheme.

A. Drive Cycles of CAEV

In this section, the modelling and simulation are carried out to evaluate the proposed control system, a series of computer simulations are performed with the MATLAB/Simulink environment for the off-line simulation analysis. Using the real-world data from CAEV, Heathrow Enterprises Ltd [15]., the two test scenarios are investigated in the following simulation tests: 1) scenario 1: CAEV travels from Terminal 5 to the car park as shown in Fig. 15 (a); 2) scenario 2: CAEV travels from the car park to Terminal 5 as shown in Fig. 16 (a). Three assumptions are applied to the simulation tests: 1) ancillary load is zero; 2) electrical machine model is ideal; 3) powertrain efficiencies are known.

B. Simulation Performance Analysis

Figs. 15 (a) to (e) show the CAEV speed profile [15], current variations, voltage variations, and SoCs of SC/batter energy storage system for the scenario 1 during acceleration and deceleration periods, respectively.

As can be expected, it is seen that the current drawn from the SC current reflected the DC-bus current is almost equal to the current drawn by the electrical machine as shown in Fig. 15 (b). Hence, the DC-bus voltage is stable as explained in Fig. 15 (c). It is also seen that SC provides the peak power and the battery provides the average power to the driving system in SC/battery energy storage system as well as the SoC shown in Figs. 15 (d) and (e). These results show that the SC/battery

energy storage system has been successfully operated in charge sustaining mode in which the SoC is maintained between the upper and lower limits.

Figs. 16 (a) to (e) show the CAEV drive cycle [15], current variations, voltage variations, and SoC of SC/batter energy storage system for the scenario 2 during acceleration and deceleration periods, respectively.

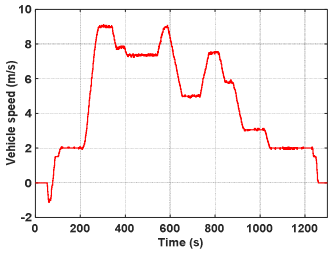

(a) CAEV drive cycle [15]

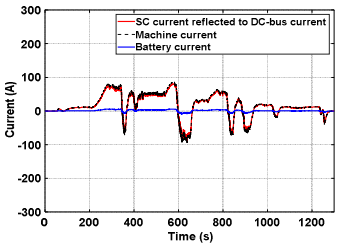

(b) Variation of current responses

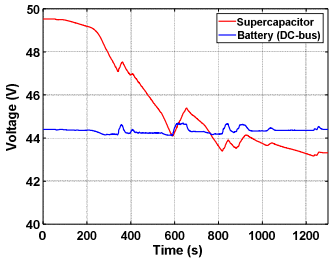

(c) Variation of voltage responses

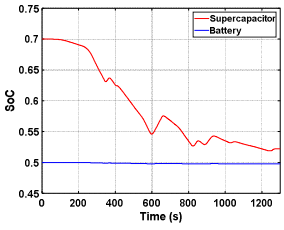

(d) SoC comparison

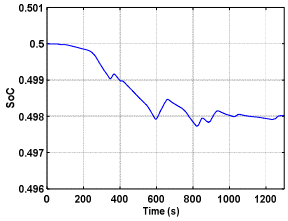

(e) Battery SoC

Fig. 15. Scenario 1.

A similar phenomenon is also found for scenario 2 when the current drawn from the SC current reflected the DC-bus current is almost equal to the current drawn by the electrical machine as shown in Fig. 16 (b), the DC-bus voltage is stable as drawn in Fig. 16 (c). The SC provides the peak power and the battery provides the average power to the driving system in SC/battery energy storage system. The comparison of SoC of SC and battery is shown in Fig. 16 (a). These results show that the DC-bus voltage is stable in which the main objective of the control approach is achieved. Moreover, since the energy from the battery is not utilized a lot, this can extend the battery life which is an advantage for the control system.

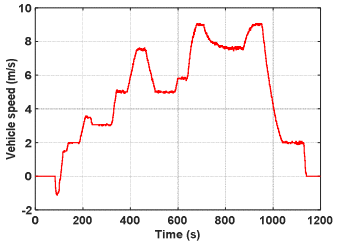

(a) CAEV drive cycle [15]

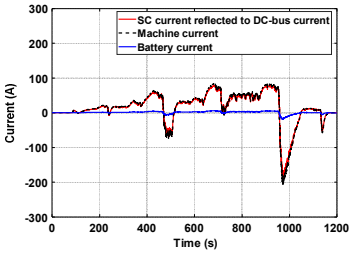

(b) Variation of current responses

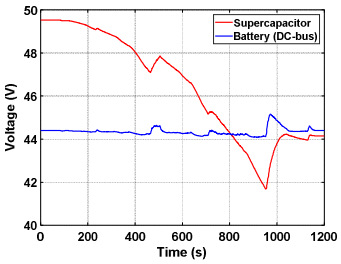

(c) Variation of voltage responses

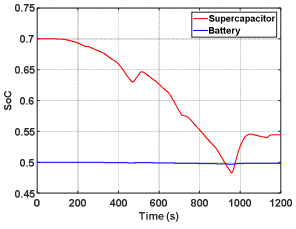

(d) SoC comparison

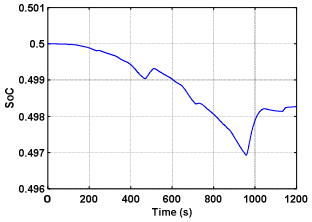

(e) Battery SoC

Fig. 16. Scenario 2.

VI. Conclusion

In conclusion, this paper has presented the design of a CAEV DC-bus voltage control system based on the hybrid SC/battery energy storage system. The control strategy has included a DC-bus voltage control system based on an energy management system and a feedforward compensator commanding the current-controlled SC and DC-DC converter.

The proposed control system has been tested by means of simulations under the CAEV driving cycle for the acceleration/deceleration operations. The simulation results show that the proposed control scheme has obvious advantages. The simulation based on the established mathematical model of the system proved that the correctness of the theory. Future work includes the study of independent Battery-SC assemblies to feed the powertrain system of CAEV. In addition, it needs to be improved by the experimental validation such as the real-time hardware in the loop (HIL) validation in the future.

ACKNOWLEDGMENT

This work was supported by Innovate UK through the Electric SuperCapacitor Integrated PODs (ESCIPODs), Project number: 103305, in collaboration with Westfield Sports Car Ltd., Heathrow Enterprises Ltd., Zap&GO Ltd., and Potenza Technology.

REFERENCES

[1] K. Hakgo,0 K. Dongwook, and S. Insoo, "Time-varying parameter adaptive vehicle speed control," *IEEE Trans. Veh. Technol.*, vol. 65, no. 2, pp. 581–588, Feb. 2015.

[2] A. Khaligh and Z. Li, "Battery, ultracapacitor, fuel cell, and hybrid energy storage systems for electric, hybrid electric, fuel cell, and plugin hybrid electric vehicles: State of the art," *IEEE Trans. Veh. Technol*., vol. 59, no. 6, pp. 2806–2814, 2010.

[3] J. Marco, and N.D. Vaughan, "Design of a reference control architecture for the energy management of electric vehicles," *Int. J. Veh. Design*, vol. 58, pp. 240-264, 2012.

[4] S. K. Kollimalla, M. K. Mishra, and N. L. Narasamma, "Design and analysis of novel control strategy for battery and supercapacitor storage system," *IEEE Trans. Sustainable Energy*, vol. 5, no. 4, pp. 1137–1144, 2014.

[5] G. Ma, M. Ghasemi and X. Song, "Integrated powertrain energy management and vehicle coordination for multiple connected hybrid electric vehicles," *IEEE Trans. Veh. Technol.*, vol. 67, no. 4, pp. 2893-2899, April 2018.

[6] W. Martinez, C. Cortes, and L. Munoz, "Sizing of ultracapacitors and batteries for a high performance electric vehicle," *IEEE International Electric Vehicle Conference*, Greenville, SC, 2012, pp. 1-6.

[7] B. Zhao, Q. Song, W. Liu, and Y.Sun, "Overview of dual-active-bridge isolated bidirectional DC–DC converter for high-frequency-link power-conversion system," *IEEE Trans. Power Electron*., pp. 4091–4106, 2014.

[8] M. Mao, Y. Liu, P. Jin, H. Huang, and L. Chang, "Energy coordinated control of hybrid battery-supercapacitor storage system in a microgrid," *4th IEEE International Symposium on Power Electronics for Distributed Generation Systems (PEDG)*, pages 1–6, July 2013.

[9] K.C. Bae, S.V. Choi, J.H. Kim, C.Y. Won, and Y.C. Jung, "LiFePO4 dynamic battery modeling for battery simulator," *Industrial Technology (ICIT), IEEE International Conference*, pp. 354–358, Feb 2014.

[10] Y. Zhu, F. Zhuo, and F. Wang, "Coordination control of lithium battery-supercapacitor hybrid energy storage system in a microgrid under unbalanced load condition," *In Power Electronics and Applications (EPE'14-ECCE Europe), 16th European Conference* on, pages 1-10, Aug 2014.

[11] C. Abbey and G. Joos, "Supercapacitor energy storage for wind energy applications," *IEEE Trans. Ind. Appl*., 43(3), pp. 769–776, May 2007.

[12] W. Li and G. Joos, "A power electronic interface for a battery supercapacitor hybrid energy storage system for wind applications," *IEEE Power Electronics Specialists Conference*, pp. 1762–1768, June 2008.

[13] X. Hu, S. Lin, S. Stanton, and W. Lian, "A foster network thermal model for HEV/EV battery modeling," *IEEE Trans. Ind. Appl*., 47(4):1692–1699, July 2011.

[14] O. Tremblay, L. A. Dessaint, and A. I. Dekkiche, "A generic battery model for the dynamic simulation of hybrid electric vehicles," *IEEE Vehicle Power and Propulsion Conference* (*VPPC*), pp. 284– 289, Sept 2007.

[15] Heathrow Enterprises Ltd. https://www.heathrow.com/